

State estimation of conceptual hydrological models using unscented Kalman filter

P. Jiang, Y. Sun and W. Bao

ABSTRACT

Unscented Kalman filter (UKF) has its origin in transforming the Gaussian random variables for nonlinear estimation and has received little attention in the context of state estimation of conceptual hydrological models. This paper introduces UKF to estimate state variables of a conceptual hydrologic model. A symmetric point approach and a scaling framework are used for performing the sample generation process of UKF. This paper investigates the application of UKF for state estimation with a synthetic case study in which both the simulated state, the true state, and the corrected state are precisely known. The results show that the use of UKF can improve the performance of both the model outputs and the state variables as the difference between the corrected trajectories and the true trajectories decreases rapidly and tends to vanish after only a few iterations. Our results and comparisons also demonstrated the capability and usefulness of UKF for state estimation in two real basins.

Key words | conceptual rainfall-runoff model, data assimilation, state estimation, streamflow forecasting, unscented Kalman filter

P. Jiang
State Key Laboratory of Hydrology-Water Resources and Hydraulic Engineering, Hohai University, Nanjing 210000, China and
Division of Hydrologic Sciences, Desert Research Institute, Las Vegas, Nevada 89119, USA

Y. Sun (corresponding author)

W. Bao
Department of Hydrology and Water Resources, Hohai University, Nanjing 210000, China
E-mail: yiqun.sun@hotmail.com

INTRODUCTION

Hydrologic models are designed to describe the rainfall-runoff physical process which is generally considered to be highly nonlinear and time-varying (Singh 1964; Pilgrim 1976). Conceptual rainfall-runoff models simplify and conceptualize these complex processes using a set of simple mathematical equations (Moradkhani *et al.* 2005a). The main purpose of these models is to predict the future evolution of the system variables. Conceptual rain-runoff models are generally reported to be robust and reliable when applied to flood forecasting (Hsu *et al.* 1995). However, it is generally accepted that the satisfactory application of such a model can be hampered by many factors including uncertainty in the inputs (Bárdossy & Das 2006; Kavetski *et al.* 2006), inadequacy of the model which generally includes uncertainty in the model structure (Gupta *et al.* 2012), uncertainty in the model parameters

(Vrugt *et al.* 2003), and uncertainty in the initial model conditions. As a result, the error correction and updating techniques have been applied to handle these problems. The Auto Regressive time series models have been used to produce improved performance of predictions by predicting the future discrepancies between the model simulations and the observations (Abrahart & See 2000; Broersen & Weerts 2005; Valipour *et al.* 2013). The sequential data assimilation (DA), which incorporates the information from observations into model simulations, has demonstrated its applicability in improving model performance (McLaughlin 2002; Kuczera *et al.* 2006; Liu & Gupta 2007). A few sequential DA techniques have been introduced in the hydrologic literature which mainly includes the dynamic identifiability analysis (Wagener *et al.* 2003), the parameter estimation approach based on the information localization (Vrugt *et al.* 2002),

and the Bayesian recursive estimation technique (BaRE) (Misirli *et al.* 2013). The standard Kalman filter is proposed to provide a recursive solution to the discrete-data linear filter problem (Kalman 1960). Several nonlinear extensions of Kalman filter such as extended Kalman filter (EKF) (Jazwinski 1970) and ensemble Kalman filter (EnKF) (Evensen 1994) have been utilized in the state estimation due to the nonlinearity of the hydrologic system. The applications of EKF in the hydrological literature have been reported by a few researchers (Entekhabi *et al.* 1994; Walker & Houser 2001). It can be considered as a 'first-order' approximation to the optimal form since EKF linearizes the nonlinear system (state equation and measurement equation) using the 'first-order' approximations (Welch & Bishop 1995). However, these approximations can introduce considerable errors, which may lead to deterioration in the performance and even divergence after a few iterations (Evensen 1994; Reichle *et al.* 2002a, 2002b). The EnKF addresses the approximation problems by incorporating an ensemble of the state, which is generated by utilizing the Monte Carlo generation (Evensen 1994; Burgers *et al.* 1998; Van Leeuwen 1999). Some applications have been seen in the hydrological literature due to its simple procedures and capability for handling the nonlinear system (Burgers *et al.* 1998; Reichle *et al.* 2002a, 2002b; Moradkhani *et al.* 2005b; Sun *et al.* 2009; Lü *et al.* 2013). In practice, implementation of EnKF may be complicated by the 'inbreeding' problem since the ensemble is updated with a gain obtained from the same ensemble in the analysis step, which can lead to underestimation of the error variances for small ensemble sizes (Van Leeuwen 1999). Particle filtering (PF) is another alternative DA technique (Arulampalam *et al.* 2002). In PF, the sequential importance sampling (SIS) is often used to achieve the optimal representation of the posterior probability distribution. For SIS, the so-called degeneracy problem typically arises, resulting in only a small number of particles being valid for the procedure. In practice, the sampling importance resampling (SIR) is proposed to handle this problem. The SIR technique has been successfully utilized to achieve state-parameter estimation of a hydrologic model (Moradkhani *et al.* 2005a). However, this resampling procedure can lead to another problem, which is known as the sample impoverishment problem (Liu & Gupta 2007).

Another well-known nonlinear extension to the Kalman filter is the unscented Kalman filter (UKF) (Julier *et al.* 1995; Julier & Uhlmann 1997). Its usefulness to nonlinear systems and efficient sampling strategy have led to extensive applications in many branches of science and engineering (St-Pierre & Gingras 2004; Wu & Smyth 2007; Kandepu *et al.* 2008; Chatzi & Smyth 2009; Chowdhary & Jategaonkar 2010; Valverde & Terzija 2011). For example, the UKF has been utilized to estimate hydraulic conductivity (Sun & Sun 2015). However, so far the UKF has received little attention in the context of state estimation of hydrological models (Liu *et al.* 2012).

In this paper, we strive to investigate the application of UKF for state estimation of hydrologic models. We seek here to: (1) introduce the basic theory of UKF and the framework of the application of UKF in state estimation in a conceptual hydrological model; and (2) evaluate its performance with a synthetic case study and real basins.

METHODOLOGY

Limitations of the Kalman filter (KF) and the nonlinear extensions

The Kalman filter is proposed to address the problem of estimating the state of a linear dynamic process which can be described by the linear stochastic equations. For the nonlinear cases, the EKF has been widely applied to these cases by linearizing the estimation around the current estimate (Welch & Bishop 1995). However, there has been a long discussion about the divergence and unstable performance of EKF (Jazwinski 1970; Gauthier *et al.* 1993; Miller *et al.* 1994; Julier *et al.* 1995). The main purpose of EKF is to propagate the expected value and the covariance of the state (the probability distribution function) through the first-order linearization of the operators for the measurement model and the state transition model. However, this can introduce considerable errors in the face of strong nonlinear relationships since the higher order partial derivatives of the functions are neglected directly. In addition, the propagation process of the distributions of the state variables can

introduce errors in the true posterior mean and covariance. This flaw can lead to unstable performance and even divergence of the EKF. Despite this main flaw, other problems such as the difficulty of calculating the Jacobian matrix also limit its applications (Da Ros & Borga 1997). The EnKF was then proposed to address the nonlinear problems mentioned above (Evensen 1994; Burgers *et al.* 1998). This technique has received much attention in the field of hydrology due to its relative simplicity and robustness when addressing the nonlinear filtering problem (Reichle *et al.* 2002a; Moradkhani *et al.* 2005b; Weerts & El Serafy 2006; Clark *et al.* 2008; Xie & Zhang 2010). The essential difference between EKF and EnKF lies in the approaches for propagating the probability distribution functions. Unlike the approximation implemented by local linearization, the EnKF utilizes a sampling strategy to propagate the probability distribution functions (Liu *et al.* 2012). While the EnKF may be a robust and popular technique for the nonlinear estimation problem, there have been some discussions about the ‘inbreeding’ problem. The main concern associated with this problem is that the gain for updating an ensemble is obtained from the same ensemble and then a modified version of EnKF named double DEnKF has been proposed to address this problem (Houtekamer & Mitchell 1998). A theoretical analysis shows that the DEnKF has only partly alleviated the problem, rather than solving it completely (Van Leeuwen 1999). Using small ensemble sizes can lead to a systematic underestimation of the error variances.

Unscented Kalman filter

The UKF was proposed as a new nonlinear extension of the Kalman filter in Julier & Uhlmann (1997). The UKF utilizes the unscented transform (UT) technique to propagate the mean and the covariance of the state, which uses a small set of weighted sample points (sigma points) to capture and propagate the expected value and covariance of the probability distributions (Julier *et al.* 2000). The main difference between this method and Monte Carlo-based methods such as EnKF and DEnKF is that the samples used in UKF are deterministic rather than random (Julier *et al.* 2000). An appealing advantage of

the UT technique is that for any inputs, the approximations are accurate to at least the second order in the face of an arbitrary nonlinear function. Moreover, for Gaussian inputs, the approximations are accurate to at least the third order. Higher accuracy can be achieved by applying different sampling strategies and changing the corresponding parameters. Various algorithms can be utilized to generate the sigma points, which include the symmetric point algorithm (Julier & Uhlmann 1997), the minimal skew simplex point algorithm (Julier & Uhlmann 2002), the spherical simplex point algorithm (Julier 2003), etc. The main distinction of these algorithms is the number of sigma points used to propagate the expected value and covariance. For an n -dimensional state (space), the symmetric point algorithm requires $2n + 1$ sigma points. However, for the minimal skew simplex point algorithm and the spherical simplex point algorithm, only $n + 2$ sigma points are required (Julier & Uhlmann 2002; Julier 2003). In addition, there are potential problems of numerical instability with the minimal skew simplex point algorithm (Julier 2003). A general framework was proposed to incorporate high order information of the system without additional computational costs while assuring the positive semi-definiteness at the same time under certain assumptions (all of the untransformed weights are non-negative) (Julier 2002).

General procedures of unscented Kalman filter

In presenting the UKF algorithm, we begin by presenting the general procedures which exclude the sampling algorithm. The equations are obtained under the assumption that both the process noise and the measurement are additive noise (with zero mean). This can significantly reduce the computational complexity (Crassidis & Junkins 2011). Let us assume that using some kind of sampling strategy we get access to a set of sigma points χ_{k-1} at time $k-1$ and the corresponding weight factors $W_i^{(c)}$ and $W_i^{(m)}$ with $i = 0, 1, \dots, n$. n is determined by the sampling approach and the dimension of state. χ_{k-1} is directly propagated through the process model:

$$\chi_{k|k-1} = f(\chi_{k-1}) \quad (1)$$

Using the weight factors, we can obtain:

$$\hat{\mathbf{X}}_k^- = \sum_{i=0}^n W_i^{(m)} \boldsymbol{\chi}_{i,k|k-1} \quad (2)$$

$$\mathbf{P}_k^- = \sum_{i=0}^n W_i^{(c)} [\boldsymbol{\chi}_{i,k|k-1} - \hat{\mathbf{X}}_k^-][\boldsymbol{\chi}_{i,k|k-1} - \hat{\mathbf{X}}_k^-]^T + \mathbf{Q} \quad (3)$$

where $\boldsymbol{\chi}_{i,k|k-1}$ represents the i th column of $\boldsymbol{\chi}_{k|k-1}$, and \mathbf{Q} represents the covariance of the process noise. To avoid additional computational costs, here we implement a resample procedure, rather than augment the sigma points vector, which means that the sigma points are recalculated using \mathbf{P}_k^- and $\hat{\mathbf{X}}_k^-$ (Wan & Van Der Merwe 2001). We will distinguish this new set of sigma points from the previous one by calling it $\boldsymbol{\chi}_{k|k-1}^r$ (hence $\boldsymbol{\chi}_{i,k|k-1}^r$). Again, $\boldsymbol{\chi}_{k|k-1}^r$ is propagated through the measurement model:

$$\boldsymbol{\gamma}_{k|k-1} = h(\boldsymbol{\chi}_{k|k-1}^r) \quad (4)$$

We obtain the expected value:

$$\hat{\mathbf{Y}}_k^- = \sum_{i=0}^n W_i^{(m)} \boldsymbol{\gamma}_{i,k|k-1} \quad (5)$$

Using the measurement \mathbf{Y}_k , the posterior state estimate can be obtained by:

$$\hat{\mathbf{X}}_k = \hat{\mathbf{X}}_k^- + \mathbf{K}(\mathbf{Y}_k - \hat{\mathbf{Y}}_k^-) \quad (6)$$

\mathbf{K} is the gain defined as:

$$\mathbf{K} = \mathbf{P}_{\hat{\mathbf{X}}_k | \hat{\mathbf{Y}}_k} \mathbf{P}_{\hat{\mathbf{Y}}_k | \hat{\mathbf{Y}}_k}^{-1} \quad (7)$$

with:

$$\mathbf{P}_{\hat{\mathbf{X}}_k | \hat{\mathbf{Y}}_k} = \sum_{i=0}^n W_i^{(c)} [\boldsymbol{\chi}_{i,k|k-1}^r - \hat{\mathbf{X}}_k^-][\boldsymbol{\gamma}_{i,k|k-1}^r - \hat{\mathbf{Y}}_k^-]^T \quad (8)$$

and:

$$\mathbf{P}_{\hat{\mathbf{Y}}_k | \hat{\mathbf{Y}}_k} = \sum_{i=0}^n W_i^{(c)} [\boldsymbol{\gamma}_{i,k|k-1}^r - \hat{\mathbf{Y}}_k^-][\boldsymbol{\gamma}_{i,k|k-1}^r - \hat{\mathbf{Y}}_k^-]^T + \mathbf{R} \quad (9)$$

where \mathbf{R} represents the covariance of the measurement noise.

Sampling algorithms and scaling framework

Several sampling algorithms have been utilized to generate the sigma points and we only mention the following: the symmetric point algorithm (Julier et al. 1995), the spherical simplex algorithm (Julier 2003) and the minimal skew simplex point algorithm (Julier & Uhlmann 2002). For the symmetric point algorithm, a set of sample points of size $2L + 1$ is used to capture and propagate the mean and the covariance for an L -dimensional space (Julier & Uhlmann 1997). All of the sample points are assigned with equal weight except the central point:

$$W_i^{(c)} = W_i^{(m)} = \begin{cases} \kappa/(L + \kappa) & i = 0 \\ 1/[2(L + \kappa)] & i = 1, 2, \dots, 2L \end{cases} \quad (10)$$

where κ represents the scaling parameter. It is recommended that the choice of κ should satisfy $L + \kappa = 3$ to achieve higher order accuracy (Julier & Uhlmann 1997). However, such a choice of κ may lead to a non-positive semidefinite estimation of $\mathbf{P}_{\hat{\mathbf{Y}}_k | \hat{\mathbf{Y}}_k}$ since κ is a negative value when the dimension of a model state is higher than 3. Then, a matrix $\boldsymbol{\chi}_{k-1}$ of $2L + 1$ vectors of sigma points (at time $k-1$) is obtained by:

$$\boldsymbol{\chi}_{k-1}^i = \begin{cases} \hat{\mathbf{X}}_{k-1} & i = 0 \\ \hat{\mathbf{X}}_{k-1} + (\sqrt{(L + \kappa)\mathbf{P}_{k-1}})^i & i = 1, 2, \dots, L \\ \hat{\mathbf{X}}_{k-1} - (\sqrt{(L + \kappa)\mathbf{P}_{k-1}})^i & i = L + 1, L + 2, \dots, 2L \end{cases} \quad (11)$$

where $\hat{\mathbf{X}}_{k-1}$ is the n -dimensional state at time $k-1$, $(\sqrt{(L + \lambda)\mathbf{P}_{k-1}})^i$ is the i th column of the matrix square root, $\boldsymbol{\chi}_{k-1}^i$ is the i th column of the matrix $\boldsymbol{\chi}_{k-1}$. To ensure the numerical stability, the Cholesky decomposition is used to obtain the matrix square root in this study.

The spherical simplex algorithm and the minimal skew simplex point algorithm can significantly reduce the number of sigma points when compared to the symmetric point algorithm (from $2L + 1$ points to $L + 2$ points) and therefore reduce the computational costs. The spherical simplex algorithm was proposed as a modified version of the minimal skew simplex point algorithm. The radius of the sphere, which bounds the sigma points, will decrease

when substituting the spherical simplex algorithm for the minimal skew simplex point algorithm. For detailed information about these algorithms, we refer to Julier & Uhlmann (2002) and Julier (2003). Despite the appealing features of UKF mentioned above, some difficulties may arise due to the fact that the radius of the sphere increases with an increase in the state dimension. The increase in the radius can introduce non-local effects. A general scaling framework was proposed to overcome these difficulties (Julier 2002). The main idea of this approach is to generate a new set of sigma points scaled by a small positive number while maintaining the second order accuracy and ensuring the positive semi-definite of the covariance if all the untransformed weight factors are non-negative. The scaling scheme is given as:

$$\chi_{k-1}^i = \hat{\mathbf{X}}_{k-1} + \alpha(\chi_{k-1}^i - \hat{\mathbf{X}}_{k-1}) \tag{12}$$

where the scaling parameter α is a small positive parameter (i.e. $0.001 \leq \alpha \leq 1$) and χ_{k-1}^i is the scaled sigma vector. After that, the weights $W_i^{(m)}$ and $W_i^{(c)}$ are adjusted accordingly (Shin & El-Sheimy 2004):

$$W_i^{(m)'} = \begin{cases} W_i^{(m)} - 1/\alpha^2 + 1 & i = 0 \\ W_i^{(m)}/\alpha^2 & i \neq 0 \end{cases} \tag{13}$$

$$W_i^{(c)'} = \begin{cases} W_i^{(m)'} + (1 + \beta - \alpha^2) & i = 0 \\ W_i^{(c)}/\alpha^2 & i \neq 0 \end{cases} \tag{14}$$

where the parameter β is utilized to incorporate the prior knowledge of the distribution. It is recommended that β is set to 2 when the distribution is assumed to be a Gaussian distribution (Julier & Uhlmann 1997). Unfortunately, there is no general criterion for choosing the best sampling algorithm and it is beyond the goal of this study to present a detailed comparison of different sampling algorithms. Hence, in this study, we use only the symmetric point algorithm and the scaling framework and we can obtain the scaling symmetric point algorithm derived in Wan & Van Der Merwe (2000). The operation of UKF is illustrated in Figure 1. ‘ T ’ represents the duration (total time steps).

Note that in practice the positive semi-definiteness of the covariance may be violated after a few iterations and then the filtering process breaks down since the Cholesky

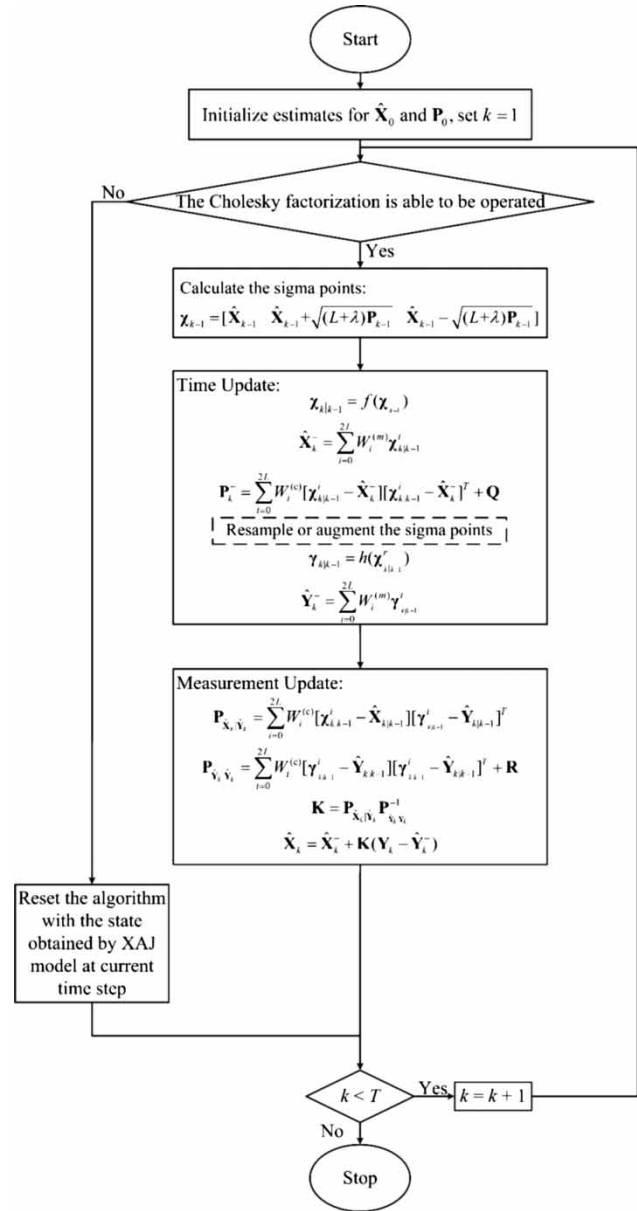


Figure 1 | Schematic for the operation of the UKF.

factorization cannot be operated. For these cases, we restart the UKF with the state obtained by the XAJ model.

CASE STUDIES

To examine the capability of the UKF for state estimation, we present a synthetic study and a real case study using a simple conceptual rainfall-runoff model. The first study mainly

serves to evaluate the performance of state estimation since we cannot get access to the actual state in the real cases. In the second case, we further applied the UKF to two real basins to test its performance and applicability. The Nash–Sutcliffe efficiency (*NSE*) (Nash & Sutcliffe 1970) and the root mean squared error (*RMSE*) were used as performance criteria in the synthetic case and the real case. The *NSE* value is a widely used measure that serves to compare the performance of a given model to the mean of the observations (Schaeffli & Gupta 2007). An *NSE* value of 1 indicates a perfect match of the model output to the observed data, while an *NSE* value of 0 means that the performance of the model is only as accurate as the mean of the observations. In this study, the *RMSE* was utilized to evaluate the performance of both the state estimation and the output estimation, while the *NSE* was only used to evaluate the output (discharge) estimation.

Hydrological model

The Xinanjiang (XAJ) rainfall-runoff model was used in this study. The XAJ model is a simple conceptual rainfall-runoff model developed by Zhao (1992) which has been widely used in most humid and semi-humid regions in China (Hu et al. 2005; Zhang et al. 2012; Shi et al. 2013; Bai et al. 2016; Jiang et al. 2017; Sun et al. 2018b). The model used in this study consists of a runoff generation module (SRP), a runoff separation module (SOR), a flow concentration module (SFC) and a channel routing module (CR) (Figure 2). Table 1 lists the physical descriptions and the units of the parameters. For detailed information about the model, we refer to Zhao (1992) and Shi et al. (2013).

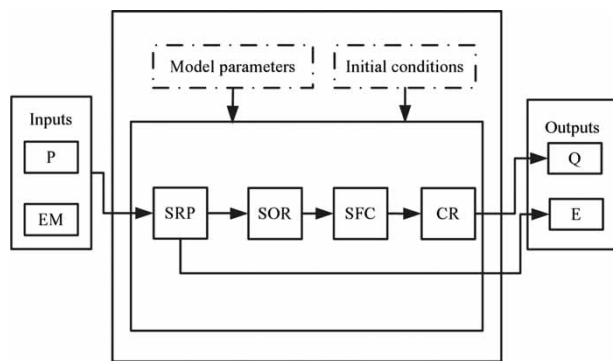


Figure 2 | Structure of the XAJ model. Note that the runoff generation module used in this study includes the three-layer evaporation module.

Table 1 | Physical descriptions of the parameters for the XAJ model

Parameter	Units	Description
WUM	mm	Areal mean tension water capacity of the upper layer
WLM	mm	Areal mean tension water capacity of the lower layer
WDM	mm	Areal mean tension water capacity of the deeper layer
B	/	Exponent of the tension water capacity distribution curve
C	/	Coefficient of deep evapotranspiration
IMP	/	Ratio of impervious area
KC	/	Ratio of potential evapotranspiration to pan evaporation
SM	mm	Areal mean free water capacity of the surface soil layer
EX	/	Exponent of the free water capacity curve
KI	/	Outflow coefficients of the free water storage to interflow
KG	/	Outflow coefficients of the free water storage to groundwater
CS	/	Recession constant of the surface water storage
CI	/	Recession constant of the interflow storage
CG	/	Recession constant of the groundwater storage
CL	/	Recession constant of the lag and route method
Lag	hour	Lag time of the lag and route method

The state vector used in this study is constructed based on the state-space model where the state variables should be sufficient to determine the future response (the future values of outputs and state variables) given the inputs and the equations describing the system (Dorf & Bishop 2011). The state vector used in this study is given as:

$$\mathbf{X} = [W \ WU \ WL \ S \ QS \ QI \ QG]^T \quad (15)$$

Descriptions of the variables in Equation (15) are presented in Table 2. The time designations are omitted for simplicity.

Synthetic case

In this study, we present a synthetic case study to demonstrate the usefulness of the UKF by using this technique and the XAJ model. This synthetic case study is similar to the synthetic

Table 2 | Descriptions of the state variables

Module	Variable	Units	Description
SRP	W	mm	Tension water storage
SRP	WU	mm	Tension water storage of the upper layer
SRP	WL	mm	Tension water storage of the lower layer
SOR	S	mm	Free water storage
SFC	QS	m^3/s	Surface flow
SFC	QI	m^3/s	Interflow
SFC	QG	m^3/s	Groundwater flow

case study used in Moradkhani *et al.* (2005a), where the synthetic study was designed to demonstrate the capability for estimating the state variables and parameters. In this study, we only focus on state estimation and therefore the main difference between these two cases is that rather than sampling the starting points for parameters, for this study, starting points for state variables were sampled from the state space. Another essential difference is that in this study the sampling process was conducted by a Latin hypercube sampling algorithm rather than a normal random sampling algorithm due to its efficient stratification properties (Helton & Davis 2003). The true values of the state and the measurement were obtained by a free run of the XAJ model using a predefined set of parameters, model inputs and starting points for the state variables. Inputs to the model are precipitation and measured pan evaporation. We utilized the mean precipitation of a real flood event, which was selected from the flood events of Qilijie basin. Qilijie basin is a Chinese humid basin with an area of 14,787 km^2 , which is located in Fujian province in southwest China. Detailed information on this flood event is presented in Table 3.

The measured pan evaporation is assumed to be a constant value (4) and the potential evaporation is evaluated by Zhao (1992):

$$EP = K \cdot EM \quad (16)$$

Table 3 | Information about the precipitation data of the synthetic flood event

Start time	End time	Duration (hour)	Sum (mm)	STD (mm)
1989/5/11 9:00	1989/6/3 8:00	552	347.3	1.12

STD represents the standard deviation.

where EM represents the measured pan evaporation (mm) and K is one of the model parameters which determines the ratio of potential evaporation with respect to the measured pan evaporation. A sample of size 20 was generated to provide the starting points for the state variables using the Latin hypercube sampling (Iman & Conover 1980; Helton & Davis 2003). Latin hypercube sampling is one of the most popular sampling strategies, which can be considered as a comprise approach between the stratified sampling and the random sampling (Helton & Davis 2003; Helton *et al.* 2006). Specifically, a random weight sample of size 20:

$$\omega_i = [\omega_{i1}, \omega_{i2}, \dots, \omega_{i7}], \quad i = 1, 2, \dots, 20 \quad (17)$$

is obtained by selecting random numbers from the intervals (0, 0.05), (0.05, 0.1), ..., (0.95, 1) since the range [0,1] is divided into 20 disjoint intervals with equal probability. For each interval, one value ω_{ij} is randomly selected. Then the 20 values for ω_{i1} are randomly paired with the values for ω_{i2} . After that, these pairs are randomly combined with the values for ω_{i3} . This process is continued until the sample of Equation (17) is obtained. For detailed descriptions of this sampling method, we refer to Helton & Davis (2003) and Helton *et al.* (2006). The upper bounds for the starting points of Equation (15) are given by:

$$\mathbf{X}_{bound} = [WM \ WUM \ WLM \ SM \ 200 \ 200 \ 200]^T \quad (18)$$

where WM is the total tension water storage capacity, WUM is the tension water storage capacity of the upper layer, WLM is the tension water storage capacity of the lower layer and SM is the free water storage capacity. These bounds (parameters) also satisfy the relationship:

$$WM = WUM + WLM + WDM \quad (19)$$

where WDM is the tension water storage capacity of the deeper layer. The true state is obtained by operating the XAJ model with the following starting points:

$$\mathbf{X}_{true} = 0.5 \mathbf{X}_{bound} \quad (20)$$

The procedures for generating the weight factors of the starting points $\mathbf{e}_i = [e_{i1}, e_{i2}, e_{i3}, e_{i4}, e_{i5}, e_{i6}, e_{i7}]$, $i = 1, 2, \dots, 20$ are illustrated by Figure 3.

As evident from Figure 3, for $j = 2, 3, 4, 5, 6$ and 7 , the starting points are directly generated by multiplying the weight values and the upper bounds. For $j = 1$, e_{i1} is the sum of the perturbed values of tension water storage of the three layers. Table 4 lists the parameters of this synthetic model.

For simplicity, the current study assumes uniform parameter fields and the area is $3,000 \text{ km}^2$. Measurement noise (additive white noise) is generated to perturb the

true measurement. Hence the measured discharge vector is obtained by:

$$\mathbf{Q}_{obs} = \mathbf{Q}_{true} + \delta\mathbf{Q} \quad (21)$$

where $\delta\mathbf{Q}$ is the measurement noise vector, \mathbf{Q}_{true} is the true measurement vector (free of noise) and \mathbf{Q}_{obs} is the measurement noise vector (with noise). The measurement noise is generated with a normal distribution with a mean of zero

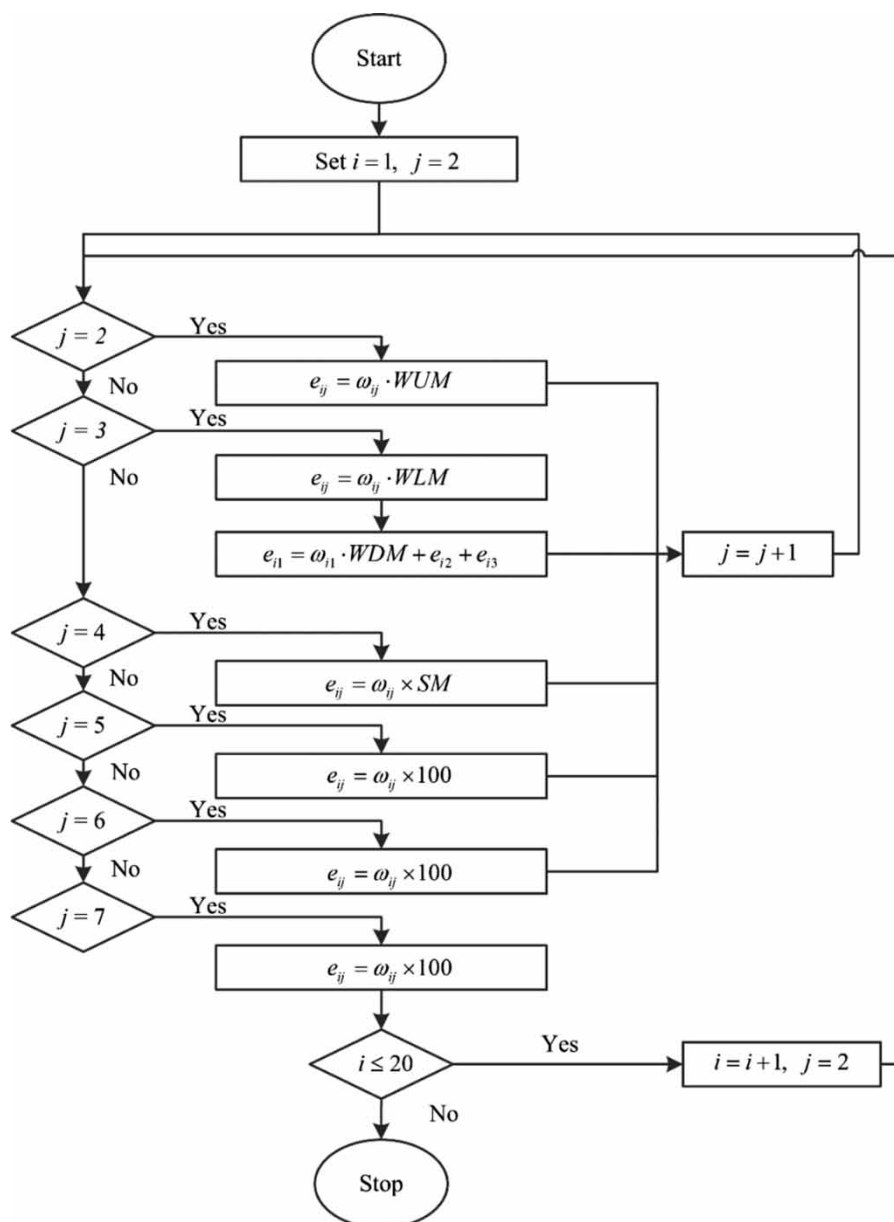


Figure 3 | Procedures for generating the weight factors of perturbed initial conditions.

Table 4 | Parameters of the synthetic model

Parameter	Value
WUM	40
WLM	100
WDM	20
B	0.4
C	0.12
IMP	0.02
KC	0.9
SM	20
EX	1.5
KI	0.3
KG	0.4
CS	0.93
CI	0.95
CG	0.98
CL	0.4
Lag	2

and the noise variance is obtained by setting $\frac{\|\delta Q\|_2}{\|Q_{true}\|_2}$ equal to 0.01. $\|\cdot\|_2$ is the 2-norm. Hence, the model state is estimated by applying the UKF with the noisy measurements, rather than the true measurements.

Real case

Study areas

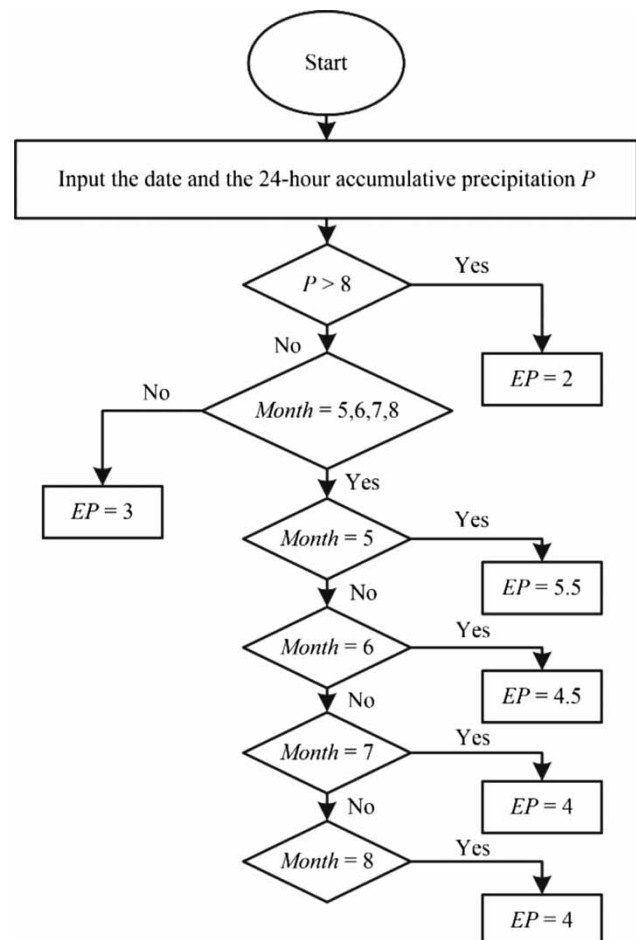
Two climatologically diverse basins were selected in this study, where snowmelt is not a dominant factor in runoff generation. Shaowu basin is located in the northwestern part of Min River basin and has an area of 2,745 km². This basin is dominated by a subtropical monsoon climate and spring and summer are the wettest seasons. We next implement this methodology to Chai River basin which is generally regarded as a sub-basin of Liao River basin. The methodology performance was tested using data from Chai River basin with an area of 1,355 km², located in one of the semi-humid regions in eastern China. Chai River basin is dominated by a temperate continental monsoon climate, resulting in abundant rainfall in summer. Thus, both a humid basin and a semi-humid basin are included in this

study. The hydrological model used in the real case study is operated in a lumped and event-based way throughout the paper. We have collected 17 flood events and 33 flood events for Shaowu basin and Chai River basin, respectively.

Data basis

The annual precipitation in Shaowu basin ranges from 1,156 to 2,423 mm for the period 1988–1999. For Shaowu basin, we used eight precipitation stations and one hydrologic station (the outlet station of Shaowu basin). The outlet station is the only available station to obtain the measured pan evaporation data of Shaowu basin and the potential evaporation for this basin is evaluated by Equation (16).

The long term mean annual precipitation of Chai River basin ranges from 494 to 1,185 mm. Precipitation inputs were based on five stations for the period 1975–2016.

**Figure 4** | Schematic for obtaining the potential evaporation for Chai River basin.

Observed runoff data was based on the Chaihepu hydrologic station, which is located at the outlet of the basin. Note that for Chai River basin, since we cannot get access to the measured pan evaporation data, the potential evaporation inputs were obtained using an empirical method in Yingpan evaporation experimental station, which is located in Liaoning, China. A brief description of this method is illustrated in Figure 4.

Figure 5 depicts the locations of two basins and the corresponding stations.

To simplify the parameter calibration problem, some of the insensitive parameters are set to plausible constants and are not further calibrated. This applies for the parameters *WUM*, *WLM*, *WDM*, *B*, *C*, *IMP* and *EX*. In addition, the sum of *KI* and *KG* is set to a fixed value (0.7) and therefore we only calibrated *KI* in this study. The ‘Lag’ *L* can be directly obtained by using the

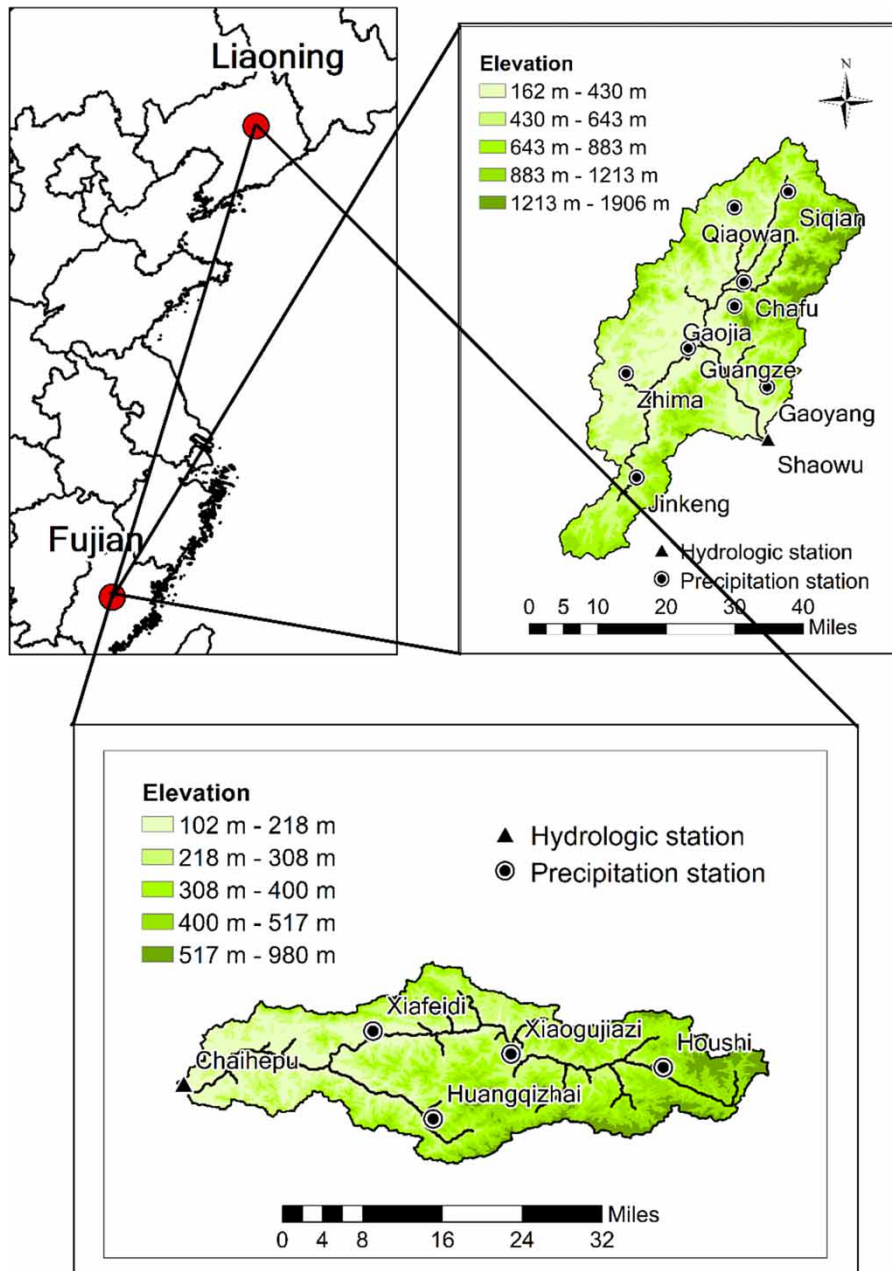


Figure 5 | Map showing locations of both basins and depicting the stations.

‘trial-and-error’ method since this parameter is a positive integer, which mainly serves to determine the ‘translation’ effect of the hydrograph. The remaining parameters were calibrated using the Particle swarm optimization algorithm (Kennedy 2011). To reduce the dimensionality of the parameters, the parameter fields are assumed uniform. The optimization process was operated by maximizing the error function, as measured by *NSE*. The optimization algorithm uses fifty particles and the value of maximum iterations (epochs) is set to 500. Table 5 lists the parameters for the two basins.

RESULTS AND DISCUSSION

Synthetic case

Figure 6 clearly shows that the corrected outputs (discharge) of all samples converge to the measurement shortly. After a few iterations (about 15 time steps), the corrected outputs are almost identical to the true measurement. Obviously, the original outputs (free of updating) differ from the measurement. This indicates that the original performance is considerably sensitive to the starting points while these perturbations can be gradually reduced by utilizing the UKF.

Table 5 | Model parameters for Shaowu basin and Chai River basin

Parameter	Shaowu basin	Chai River basin
<i>WUM</i>	20	20
<i>WLM</i>	80	100
<i>WDM</i>	20	40
<i>B</i>	0.4	0.4
<i>C</i>	0.16	0.12
<i>IMP</i>	0	0.03
<i>KC</i>	0.6	/
<i>SM</i>	10	30
<i>EX</i>	1.5	1.5
<i>KI</i>	0.3	0.58
<i>KG</i>	0.4	0.22
<i>CS</i>	0.8	0.85
<i>CI</i>	0.82	0.976
<i>CG</i>	0.97	0.999
<i>CL</i>	0.1	0.4
<i>Lag</i>	4	3

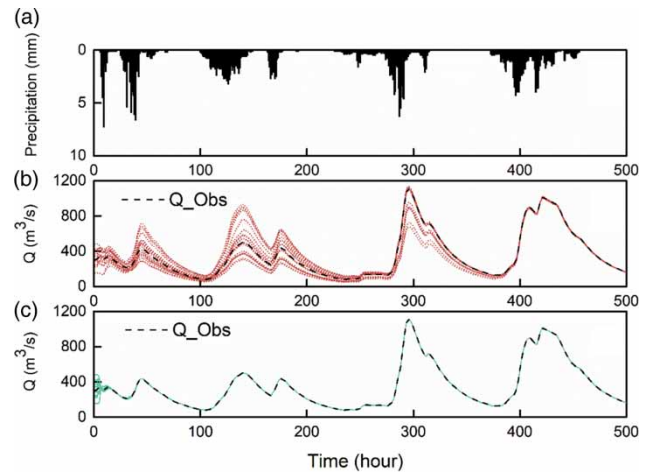


Figure 6 | Corrected results using the UKF and the original results (free of updating) for hydrograph prediction (20 sets). Dashed line represents the measured discharge. (a) Precipitation data of the synthetic study. (b) Short dot line represents the results of the original case (free of updating). (c) Solid line represents the results of the corrected case (with UKF).

Figure 7 shows a scatter plot where the original performance of the model output is plotted against the corrected performance (measured by *NSE* and *RMSE*). Throughout the paper, it is assumed that simulation using UKF results in sets suffixed by ‘_UKF’, while simulation without UKF results in sets suffixed by ‘_O’.

Figure 7 clearly shows that for all the 20 sets of starting points, using UKF has significantly improved the original performance. In our case, the *NSE* values of original case (free of updating) range from 0.7567 to 0.9975 with the mean equal to 0.9163, while the values of corrected case range from 0.9954 to 0.9997 with the mean equal to 0.9986. To evaluate the tracking capacity in detail, the results of state estimation are shown in Figure 8 (*W*, *WU* and *WL*), Figure 9 (*S*) and Figure 10 (*QS*, *QI* and *QG*). The dashed line represents the true states, the short dot line represents the original states and the solid line represents the corrected states with UKF.

As expected, the corrected state using UKF is able to track the true state since the values for the two signals (the state obtained by UKF and the actual state) match very closely. For all the state variables (except *S* and *WU*), there is a significant improvement in the performance when using the UKF. For *WU*, the performance of UKF is close to the original performance for most of the period. UKF performs better during the period 235–280. This small shift of the

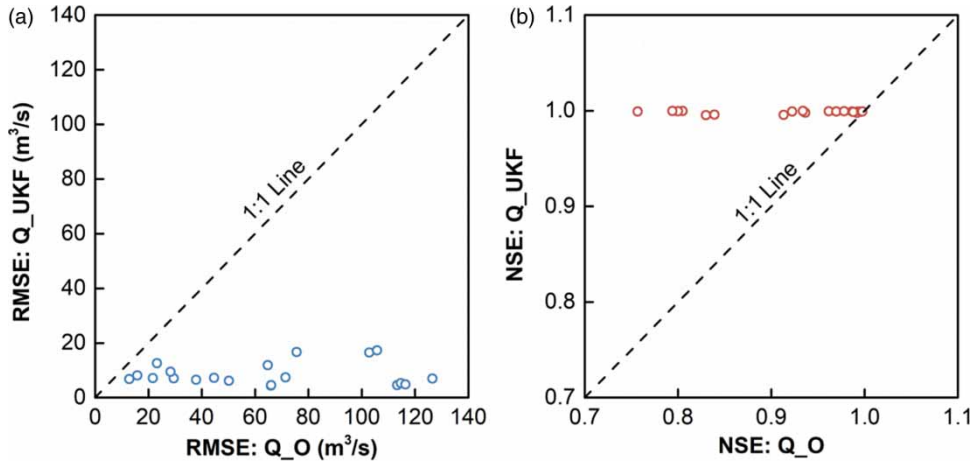


Figure 7 | Scatter plots of the original performance and the corrected performance. (a) Comparison of the result sets measured by RMSE. (b) Comparison of the result sets measured by NSE.

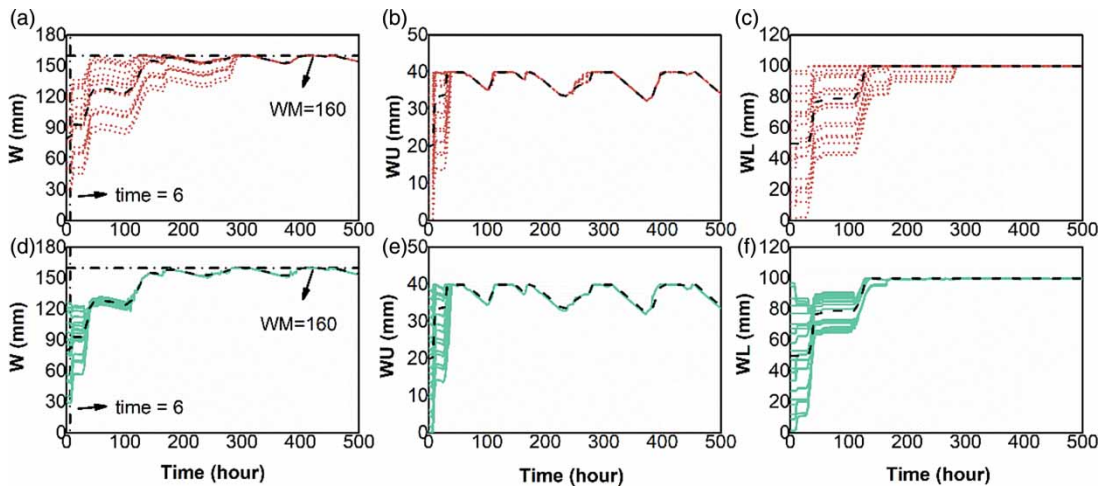


Figure 8 | Results of state estimation for the variables W , WU and WL .

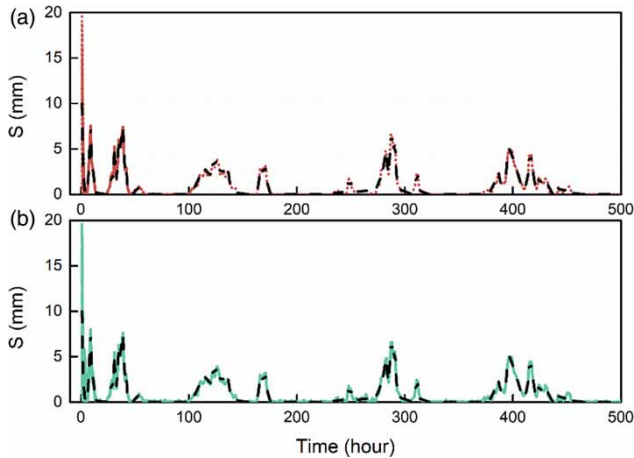


Figure 9 | Results of state estimation for the variable S .

original case is mainly caused by the model structure of the SRP module. For the XAJ model, if R is greater than 0, the total increment of tension water storage (W) is calculated by:

$$Incr_{ew} = PE - R \tag{22}$$

where PE is the net rainfall (mm), R is the runoff (mm). If $PE \leq 0$ (hence $R = 0$), the total increment is only determined by the potential evaporation and therefore the difference between the simulated value and the true value remains unchanged. Specifically, for the period 193–232, there is almost no positive net rainfall and hence the difference remains unchanged. After the time 233, the tension water storage starts to increase due to the positive net rain. Obviously,

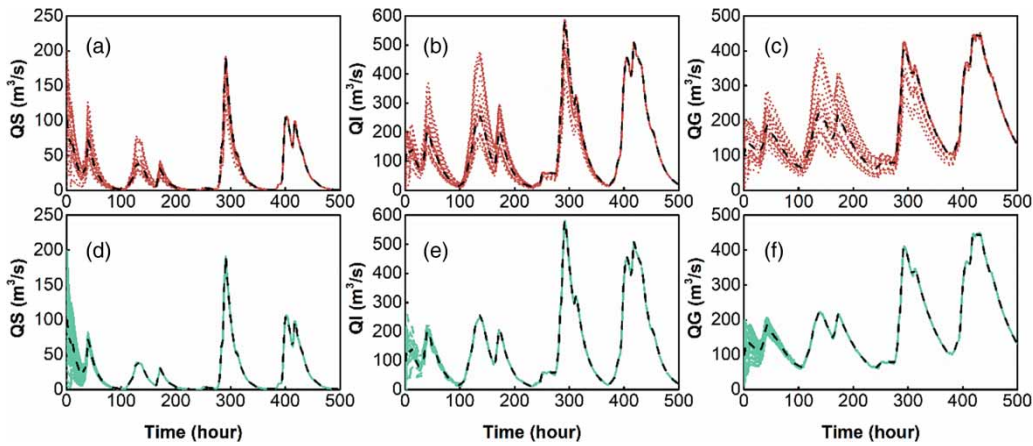


Figure 10 | Results of state estimation for the variables QS, QI and QG.

the calculated runoff for the original case tends to be smaller than the true value because during the previous period 193–232 the simulated values of tension water storage for the original case are less than the true values. Hence, $Incre_w$ in Equation (22) tends to be greater than the true value. In addition, the total increment is designed to supply the deficiency of the upper layer of the tension water storage ($WUM-WU$) in the first place, then the lower layer and the deeper layer. Therefore, some of the simulated values (WU) for the original case are greater than the true values.

However, for the variable S , both the overall trajectories (the trajectory using UKF and the original trajectory of the XAJ model) are similar to the actual trajectory (Figure 9). Actually, the overall performance of S decreases slightly when using UKF. For both cases (UKF and without UKF), the difference between the simulated values and the true values decreases rapidly and vanishes after a few iterations even without using UKF. In other words, the additional initial perturbation imposed on S is automatically eliminated. To illustrate this, we begin by writing the equation for recursively calculating S :

$$S(t) = (1 - KI - KG) \cdot S(t - 1) + (R(t) - RS(t)/FR(t)) \quad (23)$$

with:

$$FR(t) = R(t)/PE(t) \quad (24)$$

where R , RS , RI , RG and PE are the model variables (not state variables). Descriptions of these variables are presented in Table 6.

As mentioned before, the sum of the parameters KI and KG is set equal to 0.7 and therefore Equation (23) is rewritten as:

$$S(t) = 0.3 \cdot S(t - 1) + PE(t) \cdot (1 - RS(t)/R(t)) \quad (25)$$

Obviously, the difference between the true values and the simulated values will rapidly decrease and finally vanish after a few iterations because the coefficient of the first component ($0.3 \cdot S(t - 1)$) in Equation (25) is much less than one. Moreover, this may lead to a deterioration in the performance of the model output when utilizing UKF. Even though the correction of S can lead to a slight deterioration in the performance, we still do not intend to conduct UKF without updating S . The main reason for this is that the state of a system (a set of variables) should be able to determine the future response (future state and output) given the inputs and the equations describing the dynamics (Dorf & Bishop 2011). Without this variable (S),

Table 6 | Descriptions of R , RS , RI , RG and PE

Variable	Units	Description
R	mm	Runoff
RS	mm	Surface runoff
RI	mm	Interflow runoff
RG	mm	Groundwater runoff
PE	mm	Net rainfall

the variable is not sufficient to determine the future response.

An interesting observation is that the convergence time of the XAJ output is different from the convergence time of the state variables. The convergence time of the output (after about 15 time steps, see Figure 7) is much earlier than the time of soil moisture (after about 43 time steps, see Figure 8). This may suggest an important fact that the superior performance of model outputs does not necessarily imply that the performance of state variables is also satisfactory. Let us assume that the XAJ model operates without the help of UKF (free of correction) after the convergence time of the output. Clearly, the output will tend to diverge from the true trajectory after only a few iterations since there is a considerable difference between the simulated tension water storage and the true tension water storage. However, if we assume that the XAJ model operates without the UKF after the convergence time of the tension water storage, the superior performance is very likely to be maintained since the simulated state is almost identical to the true state and the only error source is assumed to be the state variables. Figure 11 shows the results of the original state and the corrected state as measured by *RMSE*.

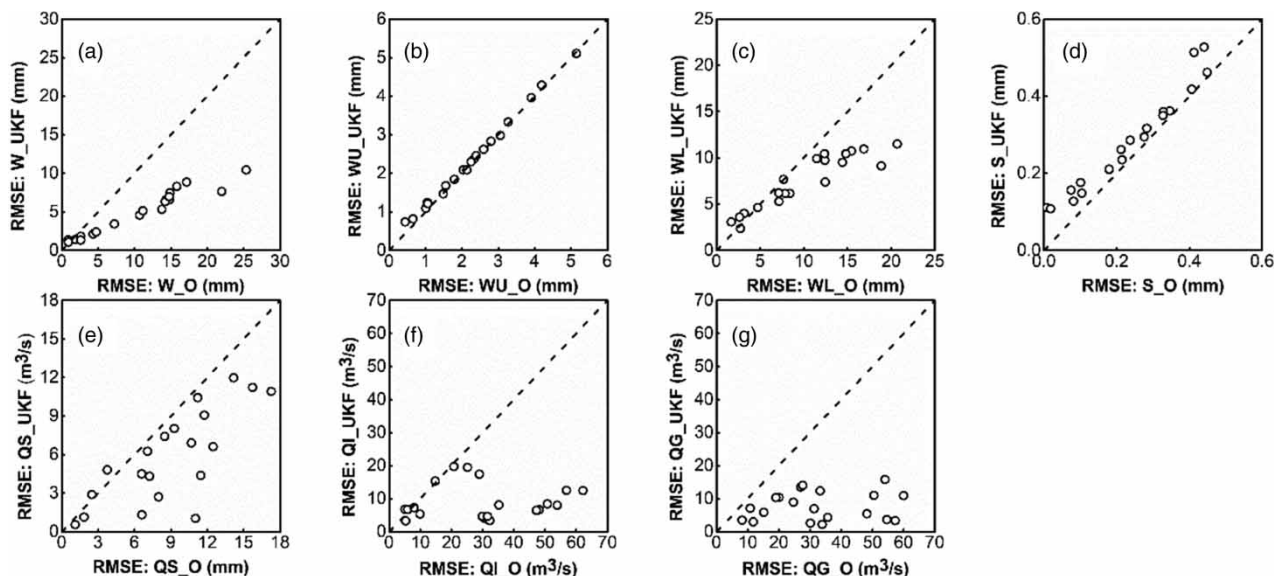


Figure 11 | Scatter plots depicting the results of simulated and observed state measured by *RMSE*. (a) Comparison of the result sets of *W*. (b) Comparison of the result sets of *WU*. (c) Comparison of the result sets of *WL*. (d) Comparison of the result sets of *S*. (e) Comparison of the result sets of *QS*. (f) Comparison of the result sets of *QI*. (g) Comparison of the result sets of *QG*.

Real cases

Figure 12 shows a scatter plot of *NSE* and *RMSE* between the ‘UKF’ performance (‘*NSE*: *Q_UKF*’ and ‘*RMSE*: *Q_UKF*’) and the original performance (‘*NSE*: *Q_O*’ and ‘*RMSE*: *Q_O*’) for Shaowu basin. Clearly, for all flood events using UKF, there is a significant increase in the performance of the model output since all the points are located in the top left of Figure 12(a) and the bottom right of Figure 12(b). *NSE* values obtained by using UKF range from 0.8702 to 0.9950 with the mean value equal to 0.9738, while for the original case the *NSE* values merely range from 0.5435 to 0.9666 with the mean value equal to 0.8242. Similar results are obtained for *RMSE* (see Figure 12(b)).

Next we apply the UKF and XAJ model in Chai River basin. Figure 13 displays a similar scatter plot.

Again, the UKF has improved the performance of the XAJ model for Chai River basin. The mean of *NSE* values has increased from 0.7821 to 0.9777, and the mean of *RMSE* values has decreased from 38.0758 to 12.2840 m³/s. Tables 7 and 8 list the results in the terms of *NSE* and *RMSE* for both basins. Therefore, these results indicate that the use of UKF has resulted in a considerable increase in the model performance for both basins. Despite the

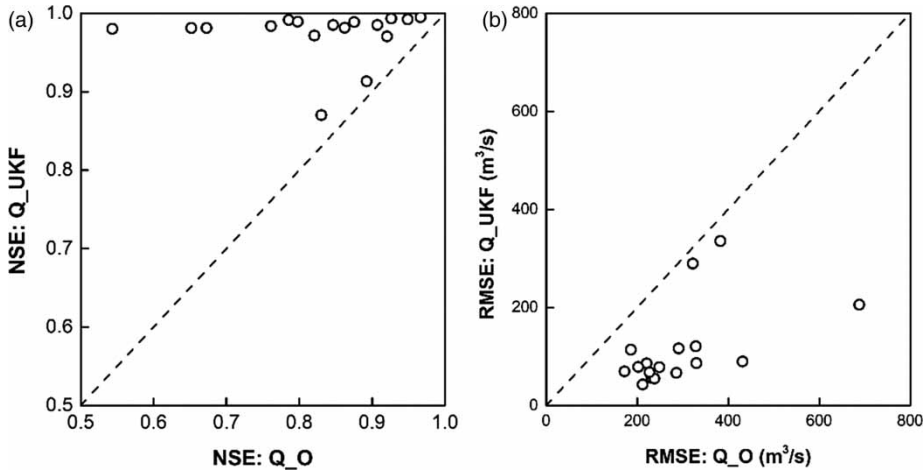


Figure 12 | Scatter plot depicting the results of UKF and the original results as measured by NSE and RMSE (Shaowu basin).

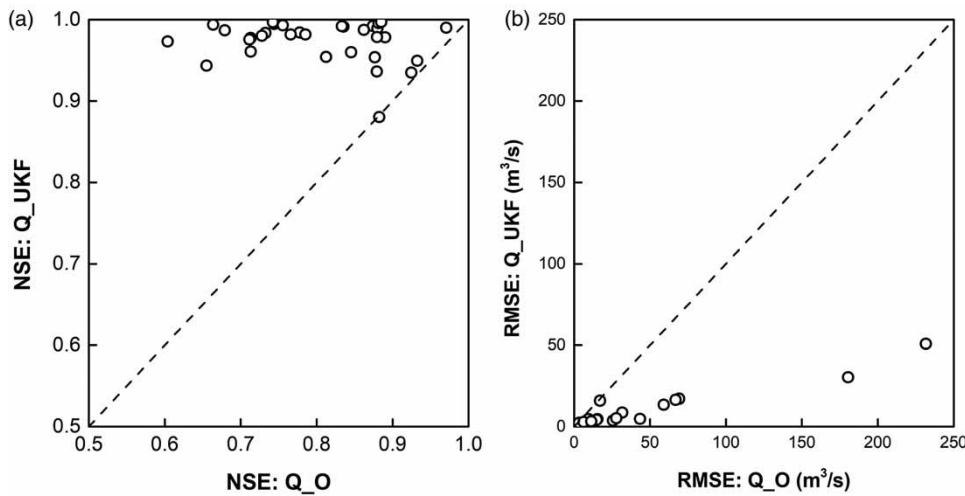


Figure 13 | Scatter plot depicting the results of UKF and the original results as measured by NSE and RMSE (Chai River basin).

satisfactory performance, note that in one of the flood events of Chai River basin there is a slight deterioration in the model performance when using UKF. This may indicate

that the attribution of the uncertainty to only the state estimation is inappropriate due to the fact that uncertainty may stem from several sources: model structure, parameters,

Table 7 | Results of the corrected performance and the original performance measured by NSE and RMSE (Shaowu basin)

	Shaowu basin			
	NSE: Q_O	NSE: Q_UKF	RMSE: Q_O (m³/s)	RMSE: Q_UKF (m³/s)
Mean	0.8242	0.9738	294.2728	115.0182
Standard Deviation	0.1144	0.0325	123.9293	83.3793
Minimum	0.5435	0.8702	172.4923	42.5896
Maximum	0.9666	0.9950	688.0272	335.2415

Table 8 | Results of the corrected performance and the original performance measured by NSE and RMSE (Chai River basin)

	Chai River basin			
	NSE: Q_O	NSE: Q_UKF	RMSE: Q_O (m³/s)	RMSE: Q_UKF (m³/s)
Mean	0.7821	0.9777	38.0758	12.2840
Standard Deviation	0.1557	0.0214	48.1152	14.7709
Minimum	0.2335	0.9349	3.2442	1.8018
Maximum	0.9247	0.9969	231.6114	53.0028

states, etc. (Sun *et al.* 1998, 2012; Clark & Vrugt 2006; Kuczera *et al.* 2006; Hendricks Franssen & Kinzelbach 2008; Renard *et al.* 2010; Sun & Sun 2015). For example, in some cases, both the uncertainty of model parameters and model state are dominant but we attribute all the uncertainty to only state uncertainty.

CONCLUSIONS

In this study, UKF was used to estimate the states of a conceptual hydrologic model. The symmetric point strategy and the general scaling framework were utilized to conduct the sampling process. A synthetic case was used to evaluate the performance of UKF for estimating the model state. The results showed that the UKF can significantly improve the accuracy of the initial conditions since the difference between the corrected trajectories and the true trajectory decreases rapidly. The application of UKF was further conducted in two real basins to demonstrate the capability of UKF in state estimation. The performance of the XAJ model has been significantly improved with the application of UKF in state estimation. It is worth noting that both state estimation and parameter estimation should be considered in the application of UKF. In this study, however, the hydrological model for the real case study was operated at event scale and the model parameters are usually considered steady during such a short period (Madsen & Skotner 2005; Bárdossy & Singh 2008). Hence, we only focus on state estimation rather than dual estimation (or joint estimation).

We would like to note that an important fact is that for real cases uncertainty may stem from several sources: model structure, parameters, states, etc. (Clark & Vrugt 2006; Kuczera *et al.* 2006; Weerts & El Serafy 2006). Considering this, it may be inappropriate to attribute all the uncertainty to only state uncertainty, which can result in model states being tweaked to unrealistic values (e.g. the estimated surface flow/runoff is negative) to compensate for other uncertainty (e.g. input uncertainty) (Sun *et al.* 2018a). This may indicate that the method ignores the physical explanation of the process of runoff generation on a hillslope. Therefore, instead of investigating correcting techniques, we should focus on implementing a better description of

the actual physical process. Such problems can lead to 'false satisfactory' situations where the right answers are obtained (e.g. considerable improvement in the output performance of hydrological modelling) for all the wrong reasons. In considering this, the choice of the right hydrological model, able to capture the main runoff generation process of the study area, should be as important as (or even more important than) a good correction method algorithm. Therefore, future work is needed to develop this method for uncertainty analysis and take other sources of uncertainty into consideration.

It is also worth noting that the computational cost of UKF can significantly increase when increasing the state dimension (Sun & Sun 2015). As a result, UKF may not be suitable for distributed hydrological models. Considering this limitation, techniques for reducing the computational cost such as the dimension reduction technique may be investigated in future studies. In addition, research aimed at improvements to the current UKF algorithm, including reliable techniques for ensuring the positive semi-definiteness of the covariance during the propagation and the sample procedure, are an open area for further research.

REFERENCES

- Abraham, R. J. & See, L. 2000 Comparing neural network and autoregressive moving average techniques for the provision of continuous river flow forecasts in two contrasting catchments. *Hydrol. Process.* **14** (11–12), 2157–2172.
- Arulampalam, M. S., Maskell, S., Gordon, N. & Clapp, T. 2002 A tutorial on particle filters for online nonlinear/non-Gaussian Bayesian tracking. *IEEE Trans. Signal Process.* **50** (2), 174–188.
- Bai, P., Liu, X., Liang, K., Liu, X. & Liu, C. 2016 A comparison of simple and complex versions of the Xinanjiang hydrological model in predicting runoff in ungauged basins. *Hydrol. Res.* **48** (5), 1282–1295.
- Bárdossy, A. & Das, T. 2006 Influence of rainfall observation network on model calibration and application. *Hydrol. Earth Syst. Sci. Discuss.* **3** (6), 3691–3726.
- Bárdossy, A. & Singh, S. 2008 Robust estimation of hydrological model parameters. *Hydrol. Earth Syst. Sci.* **12** (6), 1273–1283.
- Broersen, P. M. T. & Weerts, A. H. 2005 Automatic error correction of rainfall-runoff models in flood forecasting systems. In: *2005 IEEE Instrumentation and Measurement Technology Conference Proceedings*. IEEE, Piscataway, NJ, pp. 963–968.

- Burgers, G., Jan van Leeuwen, P. & Evensen, G. 1998 [Analysis scheme in the ensemble Kalman filter](#). *Mon. Weather Rev.* **126** (6), 1719–1724.
- Chatzi, E. N. & Smyth, A. W. 2009 [The unscented Kalman filter and particle filter methods for nonlinear structural system identification with non-located heterogeneous sensing](#). *Struct. Control Health Monit.* **16** (1), 99–123.
- Chowdhary, G. & Jategaonkar, R. 2010 [Aerodynamic parameter estimation from flight data applying extended and unscented Kalman filter](#). *Aerospace Sci. Technol.* **14** (2), 106–117.
- Clark, M. P. & Vrugt, J. A. 2006 [Unraveling uncertainties in hydrologic model calibration: addressing the problem of compensatory parameters](#). *Geophys. Res. Lett.* **33** (6), L06406.
- Clark, M. P., Rupp, D. E., Woods, R. A., Zheng, X., Ibbitt, R. P., Slater, A. G., Schmidt, J. & Uddstrom, M. J. 2008 [Hydrological data assimilation with the ensemble Kalman filter: use of streamflow observations to update states in a distributed hydrological model](#). *Adv. Water Resour.* **31** (10), 1309–1324.
- Crassidis, J. L. & Junkins, J. L. 2011 *Optimal Estimation of Dynamic Systems*. CRC Press, New York.
- Da Ros, D. & Borga, M. 1997 [Adaptive use of a conceptual model for real time flood forecasting](#). *Hydrol. Res.* **28** (3), 169–188.
- Dorf, R. C. & Bishop, R. H. 2011 *Modern Control Systems*. Pearson, Upper Saddle River, New Jersey.
- Entekhabi, D., Nakamura, H. & Njoku, E. G. 1994 [Solving the inverse problem for soil moisture and temperature profiles by sequential assimilation of multifrequency remotely sensed observations](#). *IEEE Trans. Geosci. Remote Sens.* **32** (2), 438–448.
- Evensen, G. 1994 [Sequential data assimilation with a nonlinear quasi-geostrophic model using Monte Carlo methods to forecast error statistics](#). *J. Geophys. Res. Oceans* **99** (C5), 10143–10162.
- Gauthier, P., Courtier, P. & Moll, P. 1993 [Assimilation of simulated wind lidar data with a Kalman filter](#). *Mon. Weather Rev.* **121** (6), 1803–1820.
- Gupta, H. V., Clark, M. P., Vrugt, J. A., Abramowitz, G. & Ye, M. 2012 [Towards a comprehensive assessment of model structural adequacy](#). *Water Resour. Res.* **48** (8), W08301.
- Helton, J. C. & Davis, F. J. 2003 [Latin hypercube sampling and the propagation of uncertainty in analyses of complex systems](#). *Reliab. Eng. Syst. Saf.* **81** (1), 23–69.
- Helton, J. C., Johnson, J. D., Sallaberry, C. J. & Storlie, C. B. 2006 [Survey of sampling-based methods for uncertainty and sensitivity analysis](#). *Reliab. Eng. Syst. Saf.* **91** (10), 1175–1209.
- Hendricks Franssen, H. & Kinzelbach, W. 2008 [Real-time groundwater flow modeling with the ensemble Kalman filter: joint estimation of states and parameters and the filter inbreeding problem](#). *Water Resour. Res.* **44** (9), W09408.
- Houtekamer, P. L. & Mitchell, H. L. 1998 [Data assimilation using an ensemble Kalman filter technique](#). *Mon. Weather Rev.* **126** (3), 796–811.
- Hsu, K.-L., Gupta, H. V. & Sorooshian, S. 1995 [Artificial neural network modeling of the rainfall-runoff process](#). *Water Resour. Res.* **31** (10), 2517–2530.
- Hu, C., Guo, S., Xiong, L. & Peng, D. 2005 [A modified Xinanjiang model and its application in northern China](#). *Hydrol. Res.* **36** (2), 175–192.
- Iman, R. L. & Conover, W. J. 1980 [Small sample sensitivity analysis techniques for computer models with an application to risk assessment](#). *Commun. Stat. Theory Methods* **9** (17), 1749–1842.
- Jazwinski, A. H. 1970 *Stochastic Processes and Filtering Theory*. Elsevier, New York.
- Jiang, S., Ren, L., Xu, C., Liu, S. & Yuan, F. 2017 [Quantifying multi-source uncertainties in multi-model predictions using the Bayesian model averaging scheme](#). *Hydrol. Res.* **49** (3), 954–970.
- Julier, S. J. 2002 [The scaled unscented transformation](#). In: *Proceedings of the 2002 American Control Conference* (IEEE Cat. No. CH37301), vol. 6. IEEE, Piscataway, NJ, pp. 4555–4559.
- Julier, S. J. 2003 [The spherical simplex unscented transformation](#). In: *Proceedings of the 2003 American Control Conference*, 2003, vol. 3. IEEE, Piscataway, NJ, pp. 2430–2434.
- Julier, S. J. & Uhlmann, J. K. 1997 [New extension of the Kalman filter to nonlinear systems](#). *Signal Processing, Sensor Fusion, and Target Recognition VI*. International Society for Optics and Photonics, Orlando, FL, pp. 182–194.
- Julier, S. J. & Uhlmann, J. K. 2002 [Reduced sigma point filters for the propagation of means and covariances through nonlinear transformations](#). In: *Proceedings of the 2002 American Control Conference* (IEEE Cat. No. CH37301), vol. 2. IEEE, Piscataway, NJ, pp. 887–892.
- Julier, S. J., Uhlmann, J. K. & Durrant-Whyte, H. F. 1995 [A new approach for filtering nonlinear systems](#). In: *Proceedings of the 1995 American Control Conference*, vol. 3. IEEE, Piscataway, NJ, pp. 1628–1632.
- Julier, S. J., Uhlmann, J. K. & Durrant-Whyte, H. F. 2000 [A new method for the nonlinear transformation of means and covariances in filters and estimators](#). *IEEE Trans. Automat. Contr.* **45** (3), 477–482.
- Kalman, R. E. 1960 [A new approach to linear filtering and prediction problems](#). *J. Basic Eng. Trans.* **82**, 35–45.
- Kandepu, R., Foss, B. & Imsland, L. 2008 [Applying the unscented Kalman filter for nonlinear state estimation](#). *J. Process Contr.* **18** (7), 753–768.
- Kavetski, D., Kuczera, G. & Franks, S. W. 2006 [Bayesian analysis of input uncertainty in hydrological modeling: 2. Application](#). *Water Resour. Res.* **42** (3), W03408.
- Kennedy, J. 2011 [Particle swarm optimization](#). In: *Encyclopedia of Machine Learning* (C. Sammut & G. I. Webb, eds). Springer, Boston, MA, pp. 760–766.
- Kuczera, G., Kavetski, D., Franks, S. & Thyer, M. 2006 [Towards a Bayesian total error analysis of conceptual rainfall-runoff models: characterising model error using storm-dependent parameters](#). *J. Hydrol.* **331** (1), 161–177.
- Liu, Y. & Gupta, H. V. 2007 [Uncertainty in hydrologic modeling: toward an integrated data assimilation framework](#). *Water Resour. Res.* **43** (7), W07401.

- Liu, Y., Weerts, A. H., Clark, M., Hendricks Franssen, H. J., Kumar, S., Moradkhani, H., Seo, D. J., Schwanenberg, D., Smith, P., van Dijk, A. I. J. M., van Velzen, N., He, M., Lee, H., Noh, S. J., Rakovec, O. & Restrepo, P. 2012 [Advancing data assimilation in operational hydrologic forecasting: progresses, challenges, and emerging opportunities](#). *Hydrol. Earth Syst. Sci.* **16** (10), 3863–3887.
- Lü, H., Hou, T., Horton, R., Zhu, Y., Chen, X., Jia, Y., Wang, W. & Fu, X. 2013 [The streamflow estimation using the Xinanjiang rainfall runoff model and dual state-parameter estimation method](#). *J. Hydrol.* **480** (4), 102–114.
- Madsen, H. & Skotner, C. 2005 [Adaptive state updating in real-time river flow forecasting – A combined filtering and error forecasting procedure](#). *J. Hydrol.* **308** (1–4), 302–312.
- McLaughlin, D. 2002 [An integrated approach to hydrologic data assimilation: interpolation, smoothing, and filtering](#). *Adv. Water Resour.* **25** (8), 1275–1286.
- Miller, R. N., Ghil, M. & Gauthiez, F. 1994 [Advanced data assimilation in strongly nonlinear dynamical systems](#). *J. Atmos. Sci.* **51** (8), 1037–1056.
- Misirli, F., Gupta, H. V., Sorooshian, S. & Thiemann, M. 2013 [Bayesian Recursive Estimation of Parameter and Output Uncertainty for Watershed Models, Calibration of Watershed Models](#). American Geophysical Union, Washington, DC, pp. 113–124.
- Moradkhani, H., Hsu, K.-L., Gupta, H. & Sorooshian, S. 2005a [Uncertainty assessment of hydrologic model states and parameters: sequential data assimilation using the particle filter](#). *Water Resour. Res.* **41** (5), W05012.
- Moradkhani, H., Sorooshian, S., Gupta, H. V. & Houser, P. R. 2005b [Dual state-parameter estimation of hydrological models using ensemble Kalman filter](#). *Adv. Water Resour.* **28** (2), 135–147.
- Nash, J. E. & Sutcliffe, J. V. 1970 [River flow forecasting through conceptual models part I – A discussion of principles](#). *J. Hydrol.* **10** (3), 282–290.
- Pilgrim, D. H. 1976 [Travel times and nonlinearity of flood runoff from tracer measurements on a small watershed](#). *Water Resour. Res.* **12** (3), 487–496.
- Reichle, R. H., McLaughlin, D. B. & Entekhabi, D. 2002a [Hydrologic data assimilation with the ensemble Kalman filter](#). *Mon. Weather Rev.* **130** (1), 103–114.
- Reichle, R. H., Walker, J. P., Koster, R. D. & Houser, P. R. 2002b [Extended versus ensemble Kalman filtering for land data assimilation](#). *J. Hydrometeorol.* **3** (6), 728–740.
- Renard, B., Kavetski, D., Kuczera, G., Thyer, M. & Franks, S. W. 2010 [Understanding predictive uncertainty in hydrologic modeling: the challenge of identifying input and structural errors](#). *Water Resour. Res.* **46** (5), W05521.
- Schaefli, B. & Gupta, H. V. 2007 [Do Nash values have value?](#) *Hydrol. Process.* **21** (15), 2075–2080.
- Shi, P., Zhou, M., Qu, S., Chen, X., Qiao, X., Zhang, Z. & Ma, X. 2013 [Testing a conceptual lumped model in Karst area, southwest China](#). *J. Appl. Math.* **10**, 827980.
- Shin, E. H. & El-Sheimy, N. 2004 [An unscented Kalman filter for in-motion alignment of low-cost IMUs](#). *Position Location and Navigation Symposium*. IEEE, Piscataway, NJ, pp. 273–279.
- Singh, K. P. 1964 [Nonlinear instantaneous unit-hydrograph theory](#). *J. Hydr. Div.* **90** (2), 313–350.
- St-Pierre, M. & Gingras, D. 2004 [Comparison between the unscented Kalman filter and the extended Kalman filter for the position estimation module of an integrated navigation information system](#). In: *Intelligent Vehicles Symposium*. IEEE, Piscataway, NJ, pp. 831–835.
- Sun, N. Z. & Sun, A. 2015 [Model Calibration and Parameter Estimation: for Environmental and Water Resource Systems](#). Springer, New York, NY.
- Sun, N. Z., Yang, S. L. & Yeh, W. W. G. 1998 [A proposed stepwise regression method for model structure identification](#). *Water Resour. Res.* **34** (10), 2561–2572.
- Sun, A. Y., Morris, A. & Mohanty, S. 2009 [Comparison of deterministic ensemble Kalman filters for assimilating hydrogeological data](#). *Adv. Water Resour.* **32** (2), 280–292.
- Sun, A. Y., Green, R., Swenson, S. & Rodell, M. 2012 [Toward calibration of regional groundwater models using GRACE data](#). *J. Hydrol.* **422**, 1–9.
- Sun, Y., Bao, W., Jiang, P., Ji, X., Gao, S., Xu, Y., Zhang, Q. & Si, W. 2018a [Development of multivariable dynamic system response curve method for real-time flood forecasting correction](#). *Water Resour. Res.* **54** (7), 4730–4749.
- Sun, Y., Bao, W., Jiang, P., Si, W., Zhou, J. & Zhang, Q. 2018b [Development of a regularized dynamic system response curve for real-time flood forecasting correction](#). *Water* **10** (4), 1–21.
- Valipour, M., Banihabib, M. E. & Behbahani, S. M. R. 2013 [Comparison of the ARMA, ARIMA, and the autoregressive artificial neural network models in forecasting the monthly inflow of Dez dam reservoir](#). *J. Hydrol.* **476**, 433–441.
- Valverde, G. & Terzija, V. 2011 [Unscented Kalman filter for power system dynamic state estimation](#). In: *IET Generation, Transmission and Distribution. Institution of Engineering and Technology*. IEEE, Piscataway, NJ, pp. 29–37.
- Van Leeuwen, P. J. 1999 [Comment on 'Data assimilation using an ensemble Kalman filter technique'](#). *Mon. Weather Rev.* **127** (6), 1374–1377.
- Vrugt, J. A., Bouten, W., Gupta, H. V. & Sorooshian, S. 2002 [Toward improved identifiability of hydrologic model parameters: the information content of experimental data](#). *Water Resour. Res.* **38** (12), 48–1–48-13.
- Vrugt, J. A., Gupta, H. V., Bouten, W. & Sorooshian, S. 2003 [A Shuffled Complex Evolution Metropolis algorithm for optimization and uncertainty assessment of hydrologic model parameters](#). *Water Resour. Res.* **39** (8), 1201.
- Wagener, T., McIntyre, N., Lees, M. J., Wheater, H. S. & Gupta, H. V. 2003 [Towards reduced uncertainty in conceptual rainfall-runoff modelling: dynamic identifiability analysis](#). *Hydrol. Process.* **17** (2), 455–476.

- Walker, J. P. & Houser, P. R. 2001 [A methodology for initializing soil moisture in a global climate model: assimilation of near-surface soil moisture observations](#). *J. Geophys. Res. Atmos.* **106** (D11), 11761–11774.
- Wan, E. A. & Van Der Merwe, R. 2000 The unscented Kalman filter for nonlinear estimation. In: *Proceedings of the IEEE 2000 Adaptive Systems for Signal Processing, Communications, and Control Symposium* (Cat. No.00EX373). IEEE, Piscataway, NJ, pp. 153–158.
- Wan, E. A. & Van Der Merwe, R. 2001 *The Unscented Kalman Filter. Kalman Filtering and Neural Networks*. John Wiley & Sons, NJ, pp. 221–280.
- Weerts, A. H. & El Serafy, G. Y. H. 2006 [Particle filtering and ensemble Kalman filtering for state updating with hydrological conceptual rainfall-runoff models](#). *Water Resour. Res.* **42** (9), W09403.
- Welch, G. & Bishop, G. 1995 *An Introduction to the Kalman Filter*. University of North Carolina at Chapel Hill. ACM, New York, pp. 127–132.
- Wu, M. & Smyth, A. W. 2007 [Application of the unscented Kalman filter for real-time nonlinear structural system identification](#). *Struct. Contr. Health Monit.* **14** (7), 971–990.
- Xie, X. & Zhang, D. 2010 [Data assimilation for distributed hydrological catchment modeling via ensemble Kalman filter](#). *Adv. Water Resour.* **33** (6), 678–690.
- Zhang, D., Zhang, L., Guan, Y., Chen, X. & Chen, X. 2012 [Sensitivity analysis of Xinanjiang rainfall-runoff model parameters: a case study in Lianghui, Zhejiang province](#). *China. Hydrol. Res.* **43** (1–2), 123–134.
- Zhao, R. J. 1992 The Xinanjiang model applied in China. *J. Hydrol.* **135** (1), 371–381.

First received 20 February 2018; accepted in revised form 6 November 2018. Available online 21 December 2018